

# Macrolides May Prevent Severe Acute Respiratory Syndrome Coronavirus 2 Entry into Cells: A Quantitative Structure Activity Relationship Study and Experimental Validation

Jorge Galvez,\* Riccardo Zanni, Maria Galvez-Llompart, and Jose Maria Benlloch



Cite This: <https://doi.org/10.1021/acs.jcim.0c01394>



Read Online

ACCESS |



Metrics & More

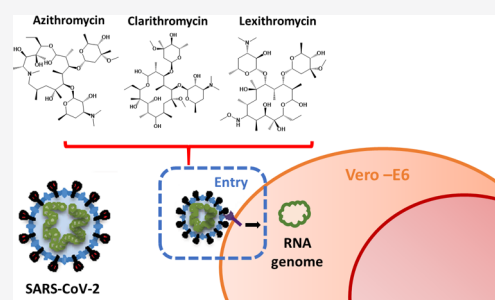


Article Recommendations



Supporting Information

**ABSTRACT:** The global pandemic caused by the emerging severe acute respiratory syndrome coronavirus 2 (SARS-CoV-2) is threatening the health and economic systems worldwide. Despite the enormous efforts of scientists and clinicians around the world, there is still no drug or vaccine available worldwide for the treatment and prevention of the infection. A rapid strategy for the identification of new treatments is based on repurposing existing clinically approved drugs that show antiviral activity against SARS-CoV-2 infection. In this study, after developing a quantitative structure activity relationship analysis based on molecular topology, several macrolide antibiotics are identified as promising SARS-CoV-2 spike protein inhibitors. To confirm the *in silico* results, the best candidates were tested against two human coronaviruses (i.e., 229E-GFP and SARS-CoV-2) in cell culture. Time-of-addition experiments and a surrogate model of viral cell entry were used to identify the steps in the virus life cycle inhibited by the compounds. Infection experiments demonstrated that azithromycin, clarithromycin, and lexitromycin reduce the intracellular accumulation of viral RNA and virus spread as well as prevent virus-induced cell death, by inhibiting the SARS-CoV-2 entry into cells. Even though the three macrolide antibiotics display a narrow antiviral activity window against SARS-CoV-2, it may be of interest to further investigate their effect on the viral spike protein and their potential in combination therapies for the coronavirus disease 19 early stage of infection.



## 1. INTRODUCTION

The world is being threatened by the emerging severe acute respiratory syndrome coronavirus 2 (SARS-CoV-2), which is responsible for the current global pandemic. This virus was recently discovered as the etiological agent responsible for the coronavirus disease 19 (COVID-19),<sup>1</sup> and in few months, it has spread over the entire world causing more than 38,000,000 confirmed cases and 1,089,000 deaths, as of October 15, 2020 (<https://covid19.who.int>). COVID-19 is characterized by nonspecific symptoms that include fever, malaise, and pneumonia, which can eventually deteriorate into more severe respiratory failure, sepsis, and death. SARS-CoV-2 is a betacoronavirus belonging to the family Coronaviridae, order Nidovirales. It is an enveloped virus with a positive-sense single-stranded RNA genome. SARS-CoV-2 enters the cell through the interaction of the viral surface glycoprotein, the spike (S) protein, with its cellular receptor, the angiotensin-converting enzyme 2 (ACE2) protein.<sup>2</sup> The transmembrane serine protease 2 (TMPRSS2) has been proposed to be responsible for the cleavage of S protein, facilitating cell entry.<sup>2</sup> Once inside the cell, the viral genome is translated into two polyproteins that are processed by the main protease 3CLpro and the papain-like protease (PLpro) producing nonstructural proteins (nsps). The viral genome is also used for replication and transcription, processes that are mediated by the viral

RNA-dependent RNA polymerase (nsp12).<sup>3</sup> Until now, remdesivir is the only antiviral compound approved by the Food and Drug Administration for the treatment of SARS-CoV-2 infection because it has been shown to reduce the hospitalization time in severe cases of COVID-19.<sup>4</sup> However, its efficacy as an antiviral agent against SARS-CoV-2 infection needs to be clearly demonstrated. Moreover, during the second and third waves of infection, even with the first doses of vaccines available, the severity of new strains of SARS-CoV-2 keeps worsening the gravity of the situation. The lack of a widely approved treatment has directed the efforts of many researchers toward the development of new compounds or repurposing existing ones. Broadly, current strategies are focused on compounds that block: (i) viral entry by affecting S-ACE2 interaction, (ii) viral nucleic acid synthesis, (iii) viral protease activity, and (iv) cytokine storm production. Many different clinically approved drugs are being currently tested as potential antivirals in SARS-CoV-2 infected patients around

Received: December 2, 2020



the world, including lopinavir, ritonavir, tocilizumab, and azithromycin, among many others (<https://ClinicalTrials.gov>). Azithromycin and other macrolides have been suggested because of their alleged role in preventing bacterial superinfection and their immunomodulatory and anti-inflammatory effects.<sup>5–9</sup> They also have demonstrated certain efficacy in reducing the severity of respiratory infections in different clinical studies.<sup>10–13</sup> Macrolides have been empirically prescribed for patients with pneumonia caused by novel coronaviruses such as SARS and MERS<sup>14–16</sup> and, more recently, SARS-CoV-2, with azithromycin attracting special attention after the release of a nonrandomized study, with methodological limitations, and an observational study, which claims that the combination of hydroxychloroquine and azithromycin achieved a higher level of SARS-CoV-2 clearance in respiratory secretions.<sup>17,18</sup> In the study, authors assessed the clinical outcomes of 20 patients with suspected COVID-19 who were treated with hydroxychloroquine (200 mg TDS for 10 days). Of these 20 patients, six additionally received azithromycin to prevent bacterial superinfection. On Day 6, 100% of patients in the combined hydroxychloroquine and azithromycin group were virologically cured; this was significantly higher than in patients receiving hydroxychloroquine alone (57.1%) ( $p < 0.001$ ). However, the efficacy of macrolides in treating SARS-CoV-2 infection based on clinical study results seems to be controversial, especially when it comes to mild and severe situations. Several authors reported results in which no significant improvement has been observed when macrolides have been administered to COVID-19 patients;<sup>19,20</sup> for example, in the study of Furtado et al.,<sup>21</sup> of 397 patients with COVID-19 confirmed, 214 were assigned to the azithromycin group and 183 to the control group with no significant improvements. It has to be reported, as stated by authors, that the entry criterion required for patients was to be on oxygen of more than 4 L/min, resulting in inclusion of a very high-risk population, with almost half of the patients on mechanical ventilation and about a quarter in shock at the baseline. With all that said, authors' main objective here is to provide new, significant insights into the potential role of macrolides in treating COVID-19 infections during the early stages. To be precise, the present quantitative structure activity relationship (QSAR) study provides new *in silico* and *in vitro* data related to azithromycin and other macrolides' capability in reducing or even impeding the entrance of the virus into hosting cells by targeting the spike receptor or by decreasing the intracellular accumulation of viral RNA and virus spread. In this report, an *in silico* study based on the construction of a molecular topology QSAR strategy<sup>22</sup> is developed, which led to the identification of a number of clinically approved macrolide antibiotics as potential agents against SARS-CoV-2 infection. The antiviral effect of macrolides is then tested in cell culture, and results suggest that azithromycin, clarithromycin, and lexithromycin display antiviral activity against SARS-CoV-2 by impeding viral entry.

## 2. RESULTS AND DISCUSSION

### 2.1. QSAR Predictive Models Based on Molecular Topology for SARS-CoV-2 Inhibitory Activity.

The first predictive model, based on discriminant analysis ( $DF_1$  function), recognizes compounds with SARS-CoV-2 inhibitory activity. The resulting equation is:

$$DF_1 = (0.203 \times \text{SPI}) - 3.866 \quad (1)$$

where  $N = 103$ , Wilks' lambda = 0.760,  $F = 32.005$ , and  $p < 0.00001$

SPI: Topological superpendentic index.

In Table S1, the value of the descriptors for the compounds composing the training set is illustrated, as well as the classification and the probability of being classified as active by the model.

Table 1 reports the classification matrix obtained for  $DF_1$ , focused on the prediction of antiviral activity against SARS-

**Table 1. Classification Matrix from Model 1**

	percent of correct classification	compounds classified as active	compounds classified as inactive
<b>training set</b>			
active group	92	11	1
inactive group	87	12	79
total	90	23	80

CoV-2. As can be seen, the model shows strong sensitivity and specificity. 90% of the active compounds and 87% of the inactive compounds have been correctly classified by the model, thus yielding an average rate of correct classification of 90% with a probability of 10% of misclassification of an inactive compound as a potential SARS-CoV-2 antiviral compound.

As for the index composing the discriminant equation, the superpendentic index (SPI) is a topological descriptor calculated from the pendent matrix, a submatrix of the distance matrix. This descriptor takes into account the branching of a molecule. In our model, it contributes positively to the discriminant function (DF), so it is expected that molecules with greater branching are related to the ability of exerting an antiviral effect against SARS-CoV-2. In Figure 1, it

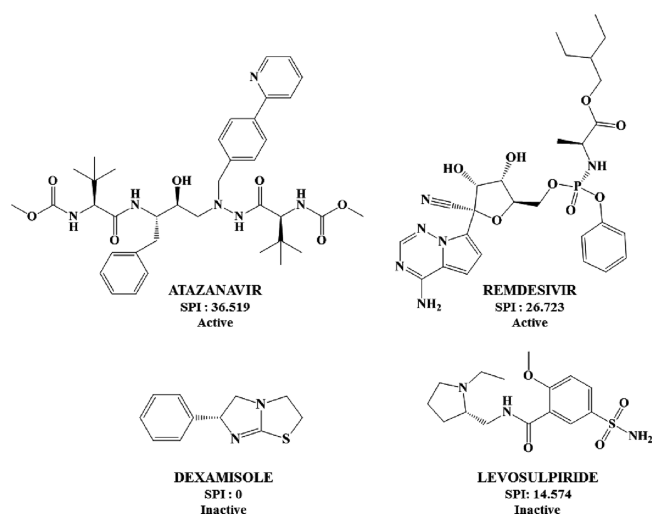


**Figure 1.** Example of SPI values for active and inactive molecules in the  $DF_1$  training set.

can be seen how the compounds with an antiviral effect against SARS-CoV-2 in general present a greater branching level in their molecular structure with respect to the inactive compounds. In fact, when analyzing the values of SPI for the training set (see Table S1), the compounds with SPI values  $>20$  are classified by  $DF_1$  as antivirals, while those with values

<20 are classified as inactive. The only exception is for arbidol, a compound that presents a lower degree of branching than the rest of the actives (Table S1).

To assess the robustness of the discriminant model,  $DF_1$  was internally validated using the leave-some-out technique (25% of the training data has been used as a test set). Because we have a limited number of active compounds in the training set ( $n = 12$ ), this technique is the best way to check the performance of the system, giving us information about model's ability to predict potential unseen data. Results are reported in Table S2 (in the Supporting Information), and as it can be seen, an average value of correct classification for the test set of 98% is obtained. Once the model has been validated, it is possible to analyze its applicability range. The PDD or pharmacological distribution diagram (Figure 2) shows a

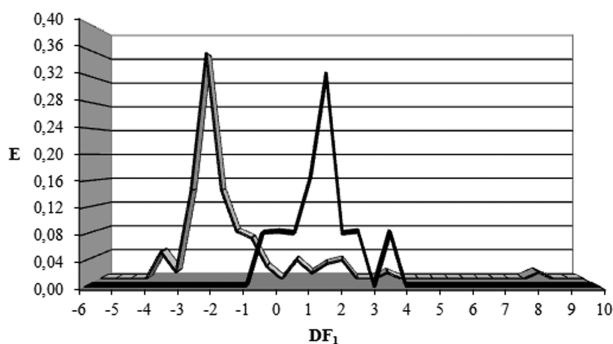


**Figure 2.** PDD for  $DF_1$ . Filled bars for the active and empty bars for the inactive.

greater expectancy of finding antiviral compounds against SARS-CoV-2 for values of the  $DF \geq -0.5$ . Therefore, when searching for potential SARS-CoV-2 inhibitors, this criterion will be taken into account.

The second predictive model ( $DF_2$ ) focuses on the identification of molecules with potential SARS-CoV-2 spike protein inhibitory activity. The resulting equation was:

$$DF_2 = (-70.180 \times MATS1s) + (79.126 \times GATS3i) - 90.475 \quad (2)$$

where  $N = 91$ ,  $\lambda = 0.3866$ ,  $F = 70.615$ ,  $p < 0.00001$ ,  $MATS1s$  is the Moran autocorrelation of lag 1 weighted by the I-state, and  $GATS3i$  is the Geary autocorrelation of lag 3 weighted by ionization potential.

In Table S3, the values of the descriptors for the different compounds of the training set as well as the classification and the probability of activity are shown.

As may be deduced from the  $DF_2$  classification matrix (Table 2), the model is capable of correctly classifying 100% of the active compounds and 96% of the inactive compounds, showing strong specificity and sensitivity.

$DF_2$  descriptors are  $MATS1s$  and  $GATS3i$ . The  $GATS3i$  descriptor or Geary autocorrelation of lag 3 weighted by the ionization potential index contributes positively to the equation, so that higher values would result in a greater probability of potential SARS-CoV-2 spike protein inhibition activity. In this specific case,  $GATS3$  is weighted by the ionization potential; hence compounds with atoms at distance 3, presenting higher ionization potentials (niclosamide or aristolochic acid), adopt higher values of this descriptor (Figure 3), while compounds that do not present atoms at

**Table 2.** Classification Matrix from Model 2

	percent of correct classification	compounds classified as active	compounds classified as inactive
<b>training set</b>			
active group	100	8	0
inactive group	96	3	80
total	98	11	81

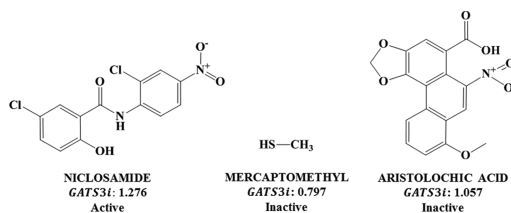


**Figure 3.** Example of  $GATS3i$  values for active and inactive molecules of the  $DF_2$  training set.

distance 3 (mercaptomethyl) present the lowest value of the training set. Compounds described as spike protein inhibitors have  $GATS3i$  values  $>1$  (Table S3), although some inactive compounds with  $GATS3i$  values  $>1$  are also found (aristolochic acid, cyano-quinocarmycin, dexecadotril, maridomycin propionate, plicamycin, and ramoplanin A2). It is to be noted that only two of them have been classified as active by the model and that plicamycin is indeed described as the spike protein inhibitor in the literature.<sup>23</sup>

$MATS1s$ , or Moran autocorrelation index of lag 1 weighted by the I-state, is a descriptor calculated by applying the Moran coefficient to a molecular graph using the intrinsic state(s) as the atomic property. In this case, it contributes negatively to the equation; therefore, in general terms, small values of this index will contribute to the inhibitory effect against virus' spike protein (Table S3). Again, using the leave-some-out technique, approximately 25% of the data set is left out as a test set, while the remaining data are used to calculate the model values. The new results are analyzed, and as shown in the Supporting Information, Table S4, the model is capable of correctly classifying almost 100% of the compounds of the test group. Once the model has been validated, the PDD is analyzed, to establish the  $DF$  value interval of activity. As illustrated in Figure 4, spike SARS-CoV-2 protein inhibitors have a higher chance to be found for  $DF_2$  value  $>0$ .

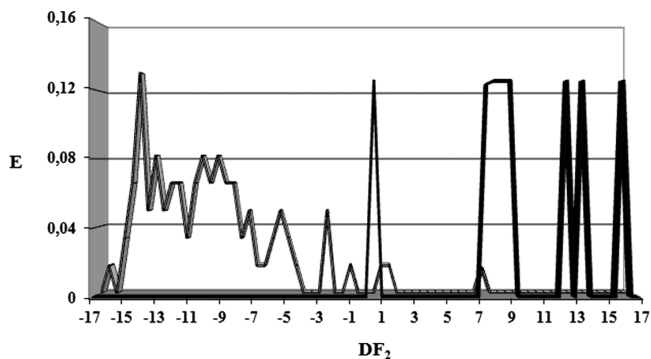


**Figure 4.** PDD for SARS-CoV-2 spike protein inhibitors (filled bars) and inactive compounds (empty bars) obtained using  $DF_2$ .

Table 3. Prediction of Antiviral and Spike Protein Inhibitory Activity for Macrolides in Clinical Use

compound	SPI	$DF_1$	P.A	MATS1s	GATS3i	$DF_2$	P.A.
azithromycin	44,37	5141	0,997	-0,164	1327	12,219	1000
clarithromycin	44,269	5121	0,997	-0,137	1257	8325	1000
erythromycin	43,725	5010	0,996	-0,149	1268	9274	1000
lexithromycin	44,836	5236	0,997	-0,149	1283	9834	1000

**2.2. Screening Macrolide Searching for Potential SARS-CoV-2 Inhibitors.** Once the QSAR models were built and validated, the mathematical pattern for molecules exhibiting a general antiviral effect and/or spike SARS-CoV-2 protein inhibitory effect is analyzed. The objective is to determine if macrolides in clinical use share the same topological pattern. Table 3 shows the descriptors calculated for the macrolides under study, as well as the value of the DFs and the probability to be classified as active by both discriminant equations. As it can be seen, the macrolides present a mathematical pattern compatible with that presented by those molecules exhibiting antiviral activity against SARS-CoV-2 ( $DF_1 > -0.5$ ); therefore,  $DF_1$  would classify them as potential anti-SARS-CoV-2 agents.

The same way as the antivirals, macrolides present a value of the SPI descriptor ( $DF_1 > 20$  (high degree of branching molecules)); therefore, the model classifies them as potential anti-SARS-CoV-2 (Figure 5).

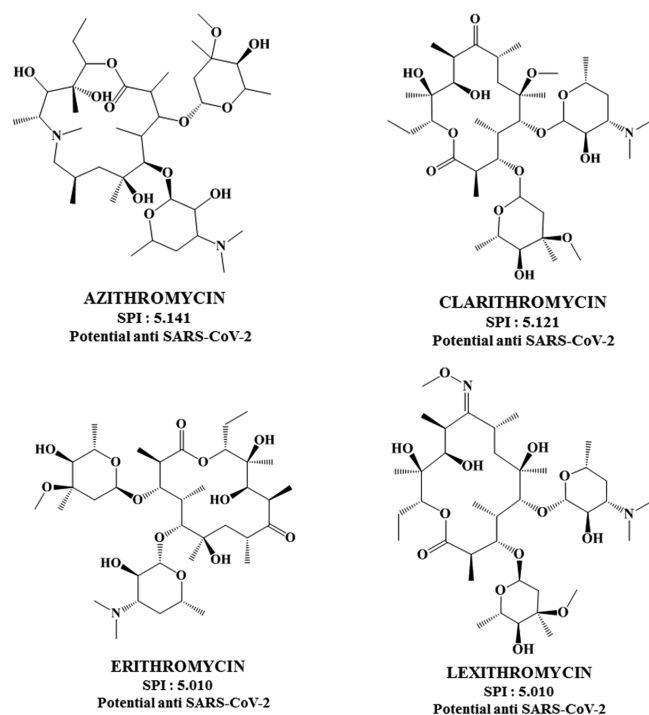


Figure 5. SPI descriptor values for all macrolides under study.

Once their potential as anti-SARS-CoV-2 is determined, the authors studied whether macrolides could exert antiviral activity through the inhibition of the virus spike protein. To do this, the mathematical pattern exhibited by the spike protein inhibitors ( $DF_2 > 0$ ) is compared with the one of macrolides. Actually, by analyzing the value of the GATS3i descriptor for macrolides, it adopts a value greater than 1 in all cases, and this is in accordance with the discriminant model outcomes for the inhibitory activity against the spike protein of

SARS-CoV-2 ( $DF_2$ ). In summary, according to the mathematical-topological models ( $DF_1$  and  $DF_2$ ), macrolides would simulate the antiviral effect through the inhibition of the SARS-CoV-2 spike protein.

**2.3. Evaluation of Macrolides as Candidate Drugs against Human Coronavirus Infection.** As a preliminary approach to confirm the antiviral potential of the aforementioned antibiotics against SARS-CoV-2, the effective concentration of the compounds capable of blocking infection by a human recombinant model coronavirus bearing a reporter gene (229E-GFP) was determined. Azithromycin, clarithromycin, and lexithromycin blocked viral infection in the absence of cytotoxicity at micromolar concentrations (Table 4). In this assay, clarithromycin showed a slightly lower potency than the other two active compounds.

Table 4. Antiviral Activity and Cytotoxicity Indexes of Selected Compounds in the 229E-GFP Infection System

compound	$EC_{50}$ ( $\mu$ M)	$EC_{90}$ ( $\mu$ M)	$CC_{50}$ ( $\mu$ M)
azithromycin	$6.1 \pm 2.4$	$18.8 \pm 2.5$	> 50
clarithromycin	$17.3 \pm 9.2$	$46.3 \pm 4.8$	> 50
erythromycin	> 50	> 50	> 50
lexithromycin	$3.0 \pm 1.4$	$16.3 \pm 6.0$	> 50

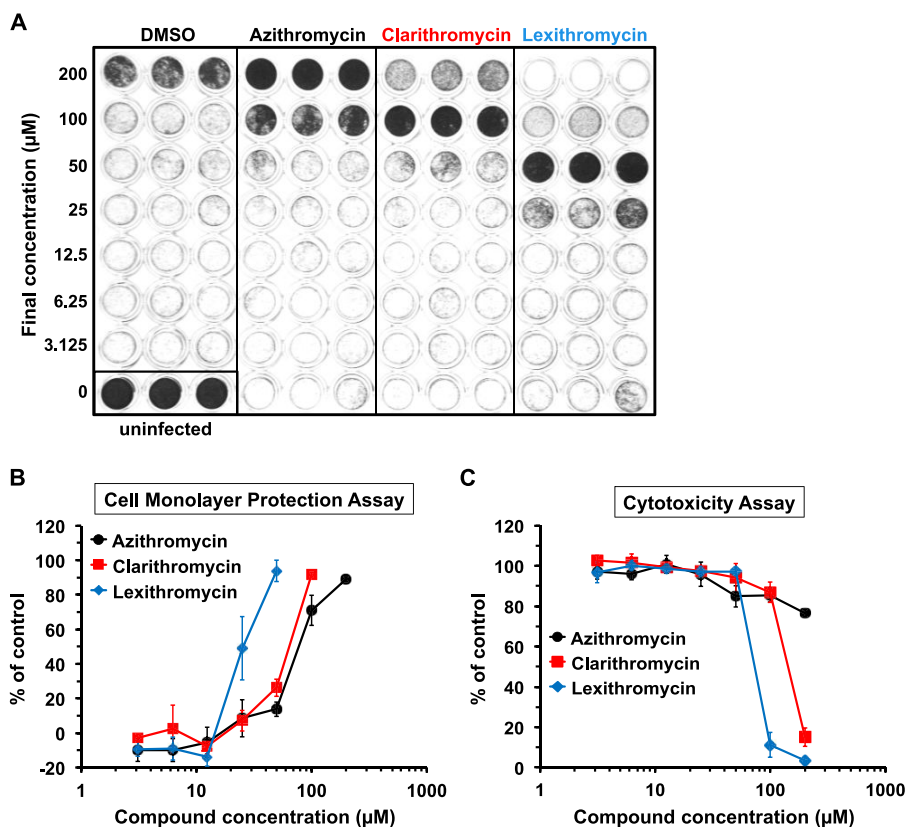
As stated in Table 4, all tested macrolides except erythromycin were active against 229E coronavirus. Hence, the inhibitory effect of clarithromycin, azithromycin, and lexithromycin against SARS-CoV-2 infection is tested to confirm their antiviral potential activity. Results show how azithromycin, clarithromycin, and lexithromycin inhibit viral infection in the absence of cytotoxicity at micromolar concentrations (Table 5). The same pattern of antiviral

Table 5. Antiviral Activity and Cytotoxicity Indexes of Selected Compounds in SARS-CoV-2

compound	$EC_{50}$ ( $\mu$ M)	$CC_{50}$ ( $\mu$ M)
azithromycin	$52 \pm 4.3$	$400 \pm 15.7$
clarithromycin	$105 \pm 8.6$	> 200
lexithromycin	$14 \pm 2.1$	$120 \pm 10.4$

potency is reproduced in both assays against 229E coronavirus and SARS-CoV-2 where lexithromycin is depicted as the most potent one followed by azithromycin. In both assays, clarithromycin was the macrolide with lower antiviral activity.

**2.4. Clarithromycin, Azithromycin, and Lexithromycin Interfere with SARS-CoV-2 Virus Infection.** Given the antiviral activity in the 229E-GFP infection system and to evaluate the antiviral potential of the antibiotics in a *bona fide* SARS-CoV-2 infection model, we performed multiple cycle infection experiments (MOI 0.001) in the presence of a range of doses of the vehicle (DMSO) or the compounds that showed antiviral potential against 229E-GFP: azithromycin, clarithromycin, and lexithromycin. All three compounds



**Figure 6.** Selected antibiotics protect from the cytopathic effect of SARS-CoV-2 infection. Vero-E6 cells were inoculated at MOI 0.001 with SARS-CoV-2 in the absence or presence of increasing doses of the compounds. (A and B) Seventy-two hours later, cells were fixed and stained with crystal violet, and the percentage of remaining biomass was estimated per well. (A) Image of a representative experiment showing protection from SARS-CoV-2 infection. (B) Quantitation of the data shown in A. Data are shown as the average and standard deviation of three biological replicates and are expressed as the relative protection in the presence of the compound as compared with the vehicle (DMSO). (C) Toxicity of compounds was determined by quantitation of crystal violet staining of uninfected Vero-E6 cells that were treated in parallel as described in panel A. Data are shown as the average and standard deviation (Mean; SD;  $n = 3$ ).

protected target cells from SARS-CoV-2 infection-induced cell death, as shown in Figure 6A,B, indicating that these compounds are capable of interfering with virus infection sufficiently to protect cells from cell death. Using this assay, it was possible to calculate an effective concentration 50 as a surrogate indicator of the relative potency of the compounds. Azithromycin showed the lowest potency as it could only protect completely the cell monolayer at 200  $\mu\text{M}$  ( $\text{EC}_{50} = 75 \mu\text{M}$ ). Interestingly, clarithromycin and lexithromycin showed increasing potency, protecting around 100% of the cell population at 100 and 50  $\mu\text{M}$ , respectively ( $\text{EC}_{50} = 60$  and 25  $\mu\text{M}$ , respectively).

The cytotoxicity study reported in Figure 6C allows appreciating how lexithromycin, clarithromycin, and azithromycin do not exert a cytotoxic effect on viral cells when used at maximum concentrations of 50, 100, and 200  $\mu\text{M}$ , respectively. Furthermore, the macrolide with a wider therapeutic window in terms of cytotoxicity seems to be azithromycin. Although this can be considered a simplification because no simple correlation between *in vitro* cytotoxicity and *in vivo* toxicity of specific drugs is possible,<sup>24</sup> indeed macrolides seem to have a relatively high margin of safety (high therapeutic index).<sup>25</sup>

As shown in Figure 7, azithromycin (100  $\mu\text{M}$ ), clarithromycin (100  $\mu\text{M}$ ), and lexithromycin (50  $\mu\text{M}$ ) reduced progeny virus production to undetectable levels, as determined by TCID<sub>50</sub> (lower limit of detection (LoD) = 100 TCID<sub>50</sub>/ml), in the absence of cytotoxicity (Figure 6C). These results

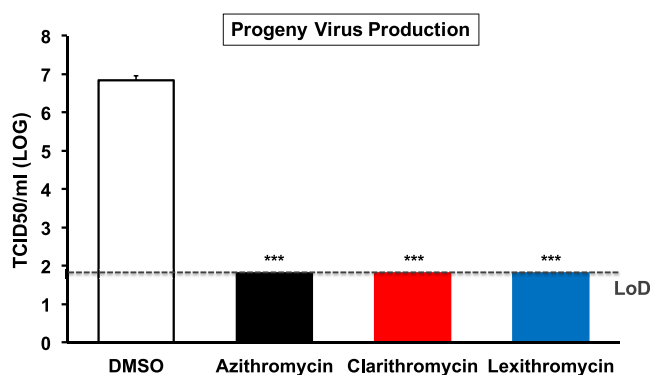


**Figure 7.** Selected antibiotics display antiviral activity against SARS-CoV-2 infection. Vero-E6 cells were inoculated at MOI 0.001 with SARS-CoV-2 in the presence of nontoxic concentrations of azithromycin (100  $\mu\text{M}$ ), clarithromycin (100  $\mu\text{M}$ ), or lexithromycin (50  $\mu\text{M}$ ). Forty-eight hours postinfection, supernatants were collected, and the infectivity titers were determined. Data are expressed as average and standard deviation of the TCID<sub>50</sub> values per ml of supernatant obtained in control and compound-treated cells. The lower LoD of the assay is represented by the discontinued gray line. Note that virus was undetectable in compound-treated conditions, despite the fact that supernatants were diluted below the effective concentrations during the titration assay.

confirm that the protective effect of the compounds is associated with the antiviral activity of the compounds.

Then, single-cycle infection experiments were performed to determine which of the steps in the virus life cycle are affected by the antibiotics. Treatment with all three compounds significantly reduced viral RNA accumulation in a dose-dependent manner, clarithromycin and lexithromycin being more potent than azithromycin (Figure 8, black bars). These

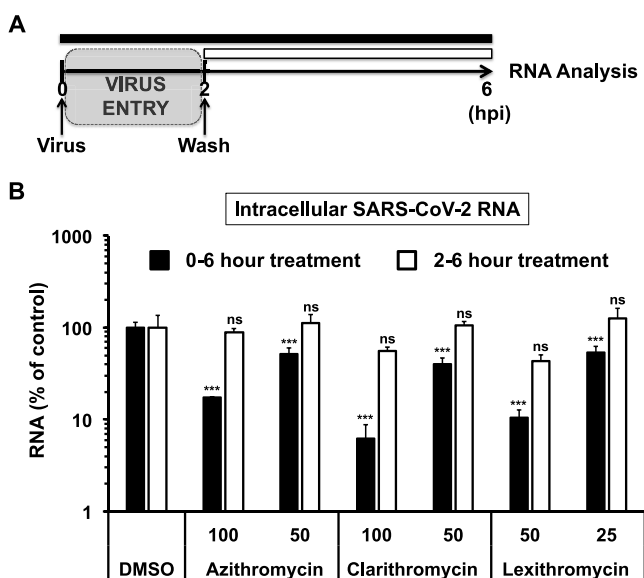


**Figure 8.** Selected antibiotics reduce intracellular SARS-CoV-2 RNA accumulation. Vero-E6 cells were inoculated at MOI 5 with SARS-CoV-2 in the presence or absence of the indicated compound concentrations. (A) Diagram explaining the experimental setup used in the experiment. Cells were treated with the compounds either at the time of virus inoculation (black bar) or 2 h thereafter (white bar), and compounds were maintained until the end of the experiment. At 6 h postinfection, cell lysates were prepared, and the RNA content was analyzed as described in the Materials and Methods section. (B) Relative intracellular SARS-CoV-2 RNA quantitation in control and compound-treated samples. Data are expressed as the average and standard deviation of biological triplicates. Note that the antiviral effect of compounds is greatly reduced when they are added after virus entry has occurred (white bars) compared to when they are added together with the virus (black bars).

results suggest that compounds inhibit early steps in the infection leading to the reduction of intracellular viral RNA. To explore this possibility, a time-of-addition experiment was performed by treating the cells 2 h after virus inoculation (white bars). As shown in Figure 9, the antiviral effect was markedly reduced when compounds were added after the virus had entered the cells, suggesting that they might interfere with virus cell entry.

**2.5. Clarithromycin, Azithromycin, and Lexithromycin Inhibit SARS-CoV-2 Spike Protein-Mediated Viral Entry.** To determine the impact of the antibiotics on viral entry, we assessed the ability of retroviral vectors pseudotyped with SARS2 S protein to enter Vero-E6 target cells in the presence of the compounds. Virus infection efficiency results suggest that all three antibiotics significantly inhibit S-mediated viral entry (Figure 9). These compounds display the expected relative effectiveness observed in the SARS-CoV-2 infection experiments lexithromycin being the most potent compound ( $EC_{50} \cong 18 \mu\text{M}$ ) and clarithromycin and azithromycin displaying comparable, lower potency ( $EC_{50} \cong 30 \mu\text{M}$ ). In parallel, entry of retroviral vectors pseudotyped with VSV G

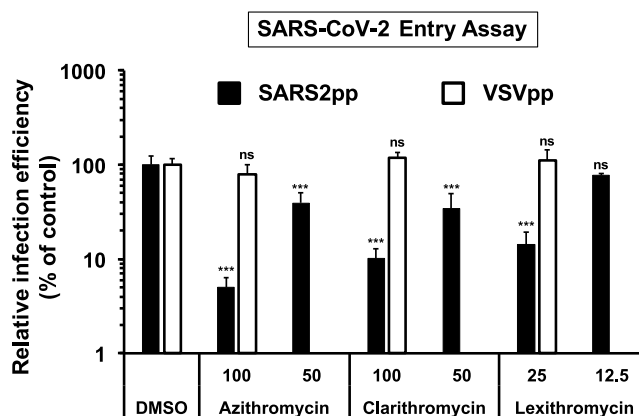


**Figure 9.** Selected antibiotics inhibit SARS-CoV-2 entry into target cells. Vero-E6 cell monolayers were inoculated with retroviral vectors pseudotyped with SARS-CoV-2 spike protein (SARS2pp) or VSV envelope glycoprotein (VSVpp) in the absence or presence of increasing doses of the compounds (i.e., 50 and 100  $\mu\text{M}$  for azithromycin and clarithromycin and 12.5 and 25  $\mu\text{M}$  for lexithromycin). Forty-eight hours postinoculation, luciferase activity was determined in whole-cell lysates. Data are expressed as relative luciferase activity values obtained in control and compound-treated cells. Data are shown as the average and standard deviation of three biological replicates.

protein (VSVpp) was not inhibited by any of the tested compounds at the highest, nontoxic concentrations, suggesting that the compounds do not interfere with reporter gene expression and that they selectively inhibit S-mediated virus entry.

### 3. CONCLUSIONS

A QSAR pattern recognition analysis employing topological and topo-chemical descriptors has been performed on antiviral and spike protein inhibitor agents against SARS-CoV-2. After the construction and validation of two discriminant models ( $DF_1$  and  $DF_2$ ), macrolides have been searched. From the computational study, some macrolides show a mathematical pattern compatible with that of antiviral and spike protein inhibitors, giving insights into the capability of these antibiotics in exerting such activity. Azithromycin, clarithromycin, erythromycin, and lexithromycin have been identified as the most promising candidates. Further *in vitro* results indicate that azithromycin, clarithromycin, and lexithromycin display antiviral behavior against human alpha- and beta-coronaviruses in cell culture infection models. According to the present experimental results, all three antibiotics seemed to be capable of reducing the SARS-CoV-2 entry into cells, suggesting that they interfere with early aspects of virus infection. Clarithromycin, azithromycin, and lexithromycin inhibit SARS-CoV-2 spike protein-mediated viral entry; however, other mechanisms for preventing viral entry cannot be excluded (considering that 229E and SARS-CoV-2 entry is mediated by different cellular receptors). This outcome is not totally unexpected as azithromycin and clarithromycin have been shown to effectively interfere with cellular endocytosis<sup>26,27</sup> and with influenza virus infection.<sup>13</sup> Clarithromycin<sup>28</sup> and azithromycin were found to be active at lower doses against HCV infection in cell culture (screen in ref.<sup>29</sup>). Thus, these compounds are not specific antivirals against SARS-CoV-2 infection. The efficacy of clarithromycin as an antiviral drug has also been tested in nonhuman primates challenged with

influenza viruses of different pathogenicity.<sup>30</sup> In that study, clarithromycin showed a modest therapeutic antiviral effect and reduction of overall pathogenesis, although it was suggested that it might contribute to amelioration of the course of the disease for its ability to reduce virus-induced inflammation.<sup>8</sup> In fact, similar to other lysosomotropic drugs (such as hydroxychloroquine and related compounds), macrolides have been previously considered in the treatment of respiratory viral infections not only for their antiviral potential, but also for their immunomodulatory role and potential reduction of virus-induced inflammation.<sup>31</sup> In summary, based on the present results, clarithromycin and lexithromycin seem to exert in cell culture a higher antiviral potency against SARS-CoV-2 than azithromycin, which is currently under clinical evaluation by several agencies as a component of therapies aimed at reducing COVID-19 severity. Despite the relatively small therapeutic window observed in cell culture, these compounds are approved for clinical use at higher dosages. Furthermore, high bioavailability at the upper and lower respiratory tract for these molecules is described.<sup>32</sup> Considering the present *in silico* and *in vitro* results, but also considering the controversial outcomes of several clinical studies showing no significant effects in reducing severe infection from SARS-CoV-2, authors consider of interest to further investigate if macrolides may be capable of preventing or reducing the gravity of COVID-19 infection during the early stages by inhibiting the spike receptor, as previously suggested for other viral respiratory infections.<sup>8,31</sup> *In vitro* results point out that three macrolide antibiotics such as azithromycin, clarithromycin, and lexithromycin exhibit antiviral activity against two distinct human coronaviruses (i.e., SARS-CoV-2 and 229E) by inhibiting entry into target cells. Our results suggest that these clinically approved antibiotics may be capable of reducing COVID-19 early infection, if administered early on after symptoms. Furthermore, and no less important, the present *in silico* strategy can be used to search new, better macrolide derivatives with improved efficacy against the SARS-CoV-2 spike receptor and to optimize the potency of the macrolides examined here.

## 4. MATERIALS AND METHODS

**4.1. Compounds.** Clinically approved compounds erythromycin (HY-B02020), clarithromycin (HY-17508), cefuroxime sodium (HY-B1256), and lexithromycin (HY-105932) were purchased from MedChemExpress (USA), while azithromycin dehydrate (PZ0007) was obtained from Merck (USA). Stock solutions were prepared in dimethyl sulfoxide (DMSO) at a final concentration of 10 mM. DMSO was used as the vehicle control in all experiments.

**4.2. In Silico Predictions Based on Molecular Topology.** **4.2.1. Compound Analysis and Molecular Descriptors.** For the construction of the first topological model, a general database of SARS-CoV-2 inhibitors is created collecting information from the literature.<sup>32–34</sup> The group of inactive compounds was created collecting molecules from the comprehensive medicinal chemistry database (CMC),<sup>35</sup> searching the literature for already described activity on SARS-CoV-2 for every molecule and taking into account different chemical and structural features to reach a coherent balance on chemical diversity between the groups (for example, to contain similar values of molecular mass, number of heteroatoms, functional groups, alicyclic or aromatic rings, etc.). The same procedure was followed for the second QSAR

equation; however this time, the training set data for the active were retrieved from references.<sup>2,36–40</sup> After a comprehensive analysis of the data set, all the molecules have been represented as a set of descriptors such as constitutional and topological descriptors. The indices were calculated with alvaDesc software version,<sup>41</sup> and their values for the selected equations for every compound included in this study (training set, external test set, and virtual screening set) are shown in the [Supporting Information](#).

**4.2.2. Modeling Techniques and Validation.** Linear discriminant analysis (LDA) allows calculating a DF, which best separates two categories or objects. When developing the QSAR models presented here, the most significant descriptors, those allowing the best separation between two categories of objects, are selected.<sup>42</sup> When selecting the descriptors, the Furnival–Wilson algorithm<sup>43,44</sup> was followed, and the Fisher–Snedecor parameter (*F*), which establishes the relevance of candidate variables, was used. Variables were chosen in a stepwise procedure according to the *F* value (to be exactly, an *F* value >1). Next, the descriptor or combination of descriptors that better explains the difference between the two groups is selected. Discriminant capability was assessed as the percentage of correct classifications in each set of compounds. Its classification criterion is based on the minimum Mahalanobis distance (the distance of each case to the mean of all cases in a category), and the quality of discrimination was evaluated using Wilks' lambda ( $\lambda$ ) parameter, which is related to the multivariate analysis of variance that tests the equality of group means for the variable in the discriminant model. The smaller is the Wilks' parameter value, the smaller is the overlap between active and inactive ( $\lambda = 0$  would mean a perfect separation between the groups). Validation of the DFs was performed using internal (*y*-randomization) validation techniques. To be exact, the leave-some-out method<sup>45</sup> consists of taking out a percentage of the data set and assigning it as a test group. The predictive model is calculated with the rest of the data set, and the leave-some-out group is analyzed. The percentage of correct classification for the test group gives insights about the reliability of the model. The software used for LDA was Statistica 9.0.<sup>46</sup>

**4.3. Potency and Cytotoxicity Indexes Using a 229E-GFP Infection Assay.** Huh7-Lunet#3 cells (kindly provided by Dr. Thommas Pietschmann; Twincore-Hannover) were maintained subconfluent in complete media [(DMEM supplemented with 10 mM HEPES, 1X nonessential amino acids (Gibco), 100 U/mL penicillin–streptomycin (Gibco), and 10% fetal bovine serum (FBS; heat-inactivated at 56 °C for 30 min)].

Huh7-Lunet#3 cells were seeded onto 96-well plates ( $1 \times 10^4$  cells/well). The day after, compound stock solutions (10 mM in DMSO) were diluted into complete cell culture media to achieve a final concentration of 100  $\mu$ M. The 100  $\mu$ M solution was serially diluted 3-fold to achieve decreasing compound concentrations. On the other hand, 229E-GFP virus stock<sup>47</sup> (kindly provided by Dr. Volker Thiel; University of Bern) was diluted in complete media to achieve a final concentration of  $3 \times 10^3$  focus forming units (FFU)/mL. One hundred microliters (100  $\mu$ L) of the virus dilution were mixed 1:1 with 100  $\mu$ L of the compound dilutions to achieve final compound concentrations in a range from 50  $\mu$ M to 22 nM and 150 infectious units (FFU) per well in a 96 well plate. One hundred  $\mu$ L of the mixture was applied onto the Huh7-Lunet#3 cell monolayer in biological replicates, and cells were cultured

for 72 h at 33 °C in a 5% CO<sub>2</sub> incubator. Cells were fixed in a 4% formaldehyde solution in PBS for 10 min at room temperature and washed twice with PBS, and individual well fluorescence was measured in a SpectraMax iD3 fluorescence plate reader (Molecular Devices). Background subtraction was performed using noninfected wells, and the signal was normalized to the average fluorescence found in vehicle (DMSO)-treated virus-infected wells. Relative infection efficiency was plotted versus compound concentration to determine the EC<sub>50</sub> and EC<sub>90</sub> (effective concentration) values. Once infection efficiency had been determined, plates were stained with a 0.1% crystal violet solution in water–methanol for 30–60 min. Then, plates were extensively washed with water and dried before 1% SDS solution in water was added to solubilize crystal violet. Absorbance was measured at 570 nm, and background was subtracted from blank wells. Relative well biomass was estimated by calculating the absorbance in each well relative to the average observed in infected cells treated with DMSO. Relative biomass was plotted versus compound concentration to determine the cytotoxic concentration (CC<sub>50</sub>) values.

**4.4. SARS-CoV-2 Infection Assays.** All high and low multiplicity of infection (MOI) experiments were performed by inoculating Vero-E6 cells seeded onto 96-well plates (2.5 × 10<sup>4</sup> cells/well) with the SARS-CoV-2 strain NL/2020 (kindly provided by Dr. R. Molenkamp, Erasmus University Medical Center Rotterdam). Cultures were maintained at 37 °C in a 5% CO<sub>2</sub> incubator for different lengths of time as indicated in each experiment. Compounds were diluted from 10 mM stock solutions in complete media containing 2% FBS to achieve the indicated final concentrations.

**4.4.1. Potency, Cytotoxicity, and Cell Monolayer Protection Assays.** Vero-E6 cell monolayers were inoculated at MOI 0.001 in the presence of a wide range of compound concentrations (from 200 to 3.125 μM) in triplicate wells. Seventy-two hours later, the cells were fixed and stained using crystal violet, as described above. Stained cells were dissolved in 1% SDS in water, and absorbance at 570 nm was used to evaluate the biomass in each well. Uninfected wells and wells infected in the presence of the vehicle (DMSO) were used as references for 100 and 0% protection.

**4.4.2. Extracellular Progeny Virus Determination.** Vero-E6 cell monolayers were inoculated at MOI 0.001 in the presence of the indicated compound concentrations. Progeny virus accumulation, present in the supernatants, was determined at 48 h postinfection by TCID<sub>50</sub> determination using the Reed and Muench method.<sup>48</sup>

**4.4.3. Intracellular Viral RNA Quantitation.** Vero-E6 cell monolayers were inoculated at MOI 5 in the presence of the indicated compound concentrations. Six hours later, cell lysates were prepared using Trizol reagent (Thermo Scientific). Viral RNA content was determined by RT-qPCR using previously validated sets of primers and probes specific for the detection of the SARS-CoV-2 E gene<sup>49</sup> and the cellular β-actin gene,<sup>50</sup> for normalization purposes. The δCt method was used for relative quantitation of the intracellular viral RNA accumulation in compound-treated cells compared to the levels in infected cells treated with DMSO, set as 100%. Time-of-addition experiments were performed by inoculating Vero-E6 cells with SARS-CoV-2 at MOI 5 in the absence of compounds. Two hours later, virus inoculum was discarded, cells were washed with PBS, and they were incubated in the presence of the indicated compound concentrations for 4 h.

Then viral RNA was extracted and analyzed as described above.

**4.5. SARS-CoV-2 Spike Protein-Pseudotyped Retroviral Vectors.** Retroviral particle production pseudotyped with different viral envelopes has previously been described.<sup>51</sup> Packaging plasmids and vesicular stomatitis virus (VSV) G protein-expressing plasmid were kindly provided by Dr. F. L. Cosset (INSERM, Lyon). SARS-CoV-2 S-expressing plasmid was obtained from Jose Maria Casanovas and Juan Garcia Arriaza (CNB-CSIC). Particles devoid of envelope glycoproteins were produced in parallel as controls.

For SARS-CoV-2 S protein-pseudotyped particle (SARS2pp) entry experiments, Vero-E6 cells (10<sup>4</sup> cells/well) were seeded onto 96-well plates the day before. Compounds were diluted in complete media [(DMEM supplemented with 10 mM HEPES, 1× nonessential amino acids (Gibco), 100 U/mL penicillin–streptomycin (Gibco), and 10% FBS (heat-inactivated at 56 °C for 30 min)] to achieve a 2× concentration. Fifty microliters (50 μL) of the SARS2pp or VSVpp retrovirus dilutions were mixed 1:1 with 50 μL of the 2x compound dilutions to achieve the desired final compound concentrations, as indicated in Figure 9. One hundred μL of the mixture was applied onto the Vero E6 cell monolayer in biological triplicates, and cells were cultured at 37 °C in a 5% CO<sub>2</sub> incubator. Forty-eight hours postinoculation, cells were lysed for luciferase activity determination using a Luciferase Assay System (Promega) and a luminometer. Relative infection values were determined by normalizing the data to the average relative light units detected in the vehicle control cells.

**4.6. Statistical Analysis.** GraphPad Prism v.5.0a software was used to perform all statistical analyses. All the results were displayed in the graphs as the mean ± standard deviation. The mean differences between multiple groups were analyzed by one-way analysis of variance followed by Dunnett's multiple comparison test. The statistical significance was set as: ns (not significant) *P* > 0.05; \* *P* < 0.05; \*\* *P* < 0.01; and \*\*\* *P* < 0.001.

## ■ ASSOCIATED CONTENT

### Supporting Information

The Supporting Information is available free of charge at <https://pubs.acs.org/doi/10.1021/acs.jcim.0c01394>.

Descriptor values, classification of compounds, and probability of activity for the training set of models 1 and 2 (Tables S1 and S3) and the leave-some-out validation test for *DF*<sub>1–2</sub> (Tables S2 and S4) (PDF)

## ■ AUTHOR INFORMATION

### Corresponding Author

Jorge Galvez – Molecular Topology and Drug Design Unit, Department of Physical Chemistry, Universitat de Valencia, Burjassot 46100, Spain; [orcid.org/0000-0003-0928-8437](https://orcid.org/0000-0003-0928-8437); Phone: +34-963544891; Email: [jorge.galvez@uv.es](mailto:jorge.galvez@uv.es)

### Authors

Riccardo Zanni – Molecular Topology and Drug Design Unit, Department of Physical Chemistry, Universitat de Valencia, Burjassot 46100, Spain; [orcid.org/0000-0002-3388-3730](https://orcid.org/0000-0002-3388-3730)

Maria Galvez-Llompарт – Molecular Topology and Drug Design Unit, Department of Physical Chemistry, Universitat

de Valencia, Burjassot 46100, Spain; Instituto de Tecnología Química, UPV-CSIC, Universidad Politécnica de Valencia, Valencia 46022, Spain; [orcid.org/0000-0002-0718-4143](https://orcid.org/0000-0002-0718-4143)

Jose Maria Benlloch – Instituto de Instrumentación para Imagen Molecular, Centro Mixto CSIC—Universitat Politècnica de València, Valencia 46022, Spain

Complete contact information is available at:  
<https://pubs.acs.org/10.1021/acs.jcim.0c01394>

### Author Contributions

Conceptualization, J.G and J.M.B.; methodology, J.G., R.Z., and M.G.L.; formal analysis, J.G., R.Z., and M.G.L.; investigation, J.G., R.Z., and M.G.L.; data curation, J.G. and J.M.B.; writing—original draft preparation, J.G, J.M.B, R.Z., and M.G.L.; and writing—review and editing, J.G and J.M.B. All authors have read and agreed to the published version of the manuscript.

### Funding

This project has been funded in part by the ERC Advanced Grant 695536 (4D-PET). This research was funded by the Spanish Ministry of Science and Innovation, grant number PIE-RD-COVID-19 ref. E202020E079 to the National Biotechnology Center (CNB-CSIC). This publication was supported by the European Virus Archive GLOBAL (EVA-GLOBAL) project that has received funding from the European Union's Horizon 2020 research and innovation program under grant agreement No 871029.

### Notes

The authors declare no competing financial interest.

### ACKNOWLEDGMENTS

We would like to thank P. Gastaminza and U. Garaigorta (Molecular and Cellular Biology Department, Centro Nacional de Biotecnología (CNB), Consejo Superior de Investigaciones Científicas (CSIC), Madrid, Spain) for obtaining all in vitro results presented in this manuscript. J. Galvez acknowledges support from the MINECO (Spanish Ministry of Economy, Industry, and Competivity) via Project: “Rational Design Of New Phytoprotection Tools” (PID2019-107464RB-C22). We are grateful to the following investigators for sharing valuable reagents: Dr. T. Pietschmann (Twincore, Hannover, Germany) for the Huh7-Lunet#3 cell line; Dr. V. Thiel (University of Bern, Bern, Switzerland) for the 299E-GFP virus; Dr. R. Molenkamp (Erasmus University Medical Center, Rotterdam, Netherlands; participant of the EVA-GLOBAL project) for the SARS-CoV-2 strain NL/2020 virus; Dr. F.L. Closset (Inserm, Lyon, France) for the retrovirus packing plasmid system and the VSV G protein-expressing plasmid; and Drs. J. M. Casanovas and J. García-Arriaza (CNB-CSIC, Madrid, Spain) for the SARS-CoV-2 S-expressing plasmid.

### REFERENCES

- (1) Zhu, N.; Zhang, D.; Wang, W.; Li, X.; Yang, B.; Song, J.; Zhao, X.; Huang, B.; Shi, W.; Lu, R. A novel coronavirus from patients with pneumonia in China. *N. Engl. J. Med.* **2020**, *382*, 727–733.
- (2) Hoffmann, M.; Kleine-Weber, H.; Schroeder, S.; Krüger, N.; Herrler, T.; Erichsen, S.; Schiergens, T. S.; Herrler, G.; Wu, N.; Nitsche, A. SARS-CoV-2 cell entry depends on ACE2 and TMPRSS2 and is blocked by a clinically proven protease inhibitor. *Cell* **2020**, *181*, 271–280.e8.
- (3) Fehr, A. R.; Perlman, S. Coronaviruses: an overview of their replication and pathogenesis. *Coronaviruses* **2015**, *1282*, 1–23.

- (4) Beigel, J. H.; Tomashek, K. M.; Dodd, L. E.; Mehta, A. K.; Zingman, B. S.; Kalil, A. C.; Hohmann, E.; Chu, H. Y.; Luetkemeyer, A.; Kline, S.; Lopez de Castilla, D.; Finberg, R. W.; Dierberg, K.; Tapson, V.; Hsieh, L.; Patterson, T. F.; Paredes, R.; Sweeney, D. A.; Short, W. R.; Touloumi, G.; Lye, D. C.; Ohmagari, N.; Oh, M. D.; Ruiz-Palacios, G. M.; Benfield, T.; Fätkenheuer, G.; Kortepeter, M. G.; Atmar, R. L.; Creech, C. B.; Lundgren, J.; Babiker, A. G.; Pett, S.; Neaton, J. D.; Burgess, T. H.; Bonnett, T.; Green, M.; Makowski, M.; Osinusi, A.; Nayak, S.; Lane, H. C. ACTT-1 Study Group Members. Remdesivir for the treatment of COVID-19: final report. *N. Engl. J. Med.* **2020**, *383*, 1813–1826.

- (5) Poddighe, D.; Aljofan, M. Clinical evidences on the antiviral properties of macrolide antibiotics in the COVID-19 era and beyond. *Antivir. Chem. Chemother.* **2020**, *28*, No. 204020662096171.

- (6) Amsden, G. W. Anti-inflammatory effects of macrolides—an underappreciated benefit in the treatment of community-acquired respiratory tract infections and chronic inflammatory pulmonary conditions? *J. Antimicrob. Chemother.* **2005**, *55*, 10–21.

- (7) Kanoh, S.; Rubin, B. K. Mechanisms of action and clinical application of macrolides as immunomodulatory medications. *Clin. Microbiol. Rev.* **2010**, *23*, 590–615.

- (8) Min, J.-Y.; Jang, Y. J. Macrolide therapy in respiratory viral infections. *Mediators Inflamm.* **2012**, *2012*, No. 649570.

- (9) Lin, S.-J.; Kuo, M.-L.; Hsiao, H.-S.; Lee, P.-T. Azithromycin modulates immune response of human monocyte-derived dendritic cells and CD4 T cells. *Int. Immunopharmacol.* **2016**, *40*, 318–326.

- (10) Tahan, F.; Ozcan, A.; Koc, N. Clarithromycin in the treatment of RSV bronchiolitis: a double-blind, randomised, placebo-controlled trial. *Eur. Respir. J.* **2007**, *29*, 91–97.

- (11) Suzuki, T.; Yamaya, M.; Sekizawa, K.; Hosoda, M.; Yamada, N.; Ishizuka, S.; Yoshino, A.; Yasuda, H.; Takahashi, H.; Nishimura, H. Erythromycin inhibits rhinovirus infection in cultured human tracheal epithelial cells. *Am. J. Respir. Crit. Care Med.* **2002**, *165*, 1113–1118.

- (12) Jang, Y. J.; Kwon, H. J.; Lee, B. J. Effect of clarithromycin on rhinovirus-16 infection in A549 cells. *Eur. Respir. J.* **2006**, *27*, 12–19.

- (13) Yamaya, M.; Shinya, K.; Hatachi, Y.; Kubo, H.; Asada, M.; Yasuda, H.; Nishimura, H.; Nagatomi, R. Clarithromycin inhibits type a seasonal influenza virus infection in human airway epithelial cells. *J. Pharmacol. Exp. Ther.* **2010**, *333*, 81–90.

- (14) Lee, N.; Wong, C.; Chan, M. C.; Yeung, E. S.; Tam, W. W.; Tsang, O. T.; Choi, K.; Chan, P. K.; Kwok, A.; Lui, G. C. Anti-inflammatory effects of adjunctive macrolide treatment in adults hospitalized with influenza: a randomized controlled trial. *Antiviral Res.* **2017**, *144*, 48–56.

- (15) Bermejo-Martin, J. F.; Kelvin, D. J.; Eiros, J. M.; Castrodeza, J.; De Lejarazu, R. O. Macrolides for the treatment of severe respiratory illness caused by novel H1N1 swine influenza viral strains. *J. Infect. Dev. Ctries.* **2009**, *3*, 159–161.

- (16) Lendermon, E. A.; Coon, T. A.; Bednash, J. S.; Weathington, N. M.; McDyer, J. F.; Mallampalli, R. K. Azithromycin decreases NALP3 mRNA stability in monocytes to limit inflammasome-dependent inflammation. *Respir. Res.* **2017**, *18*, 1–8.

- (17) Gautret, P.; Lagier, J.; Parola, P.; Meddeb, L.; Mailhe, M.; Doudier, B.; Courjon, J.; Giordanengo, V.; Vieira, V. E.; Dupont, H. T. Hydroxychloroquine and azithromycin as a treatment of COVID-19: results of an open-label non-randomized clinical trial. *Int. J. Antimicrob. Agents* **2020**, *56*, No. 105949.

- (18) Gautret, P.; Lagier, J.; Parola, P.; Meddeb, L.; Sevestre, J.; Mailhe, M.; Doudier, B.; Aubry, C.; Amrane, S.; Seng, P. Clinical and microbiological effect of a combination of hydroxychloroquine and azithromycin in 80 COVID-19 patients with at least a six-day follow up: a pilot observational study. *Travel Med. Infect. Dis.* **2020**, *34*, No. 101663.

- (19) Cavalcanti, A. B.; Zampieri, F. G.; Rosa, R. G.; Azevedo, L. C.; Veiga, V. C.; Avezum, A.; Damiani, L. P.; Marcadenti, A.; Kawano-Dourado, L.; Lisboa, T. Hydroxychloroquine with or without Azithromycin in Mild-to-Moderate Covid-19. *N. Engl. J. Med.* **2020**, *383*, 2041–2052.

- (20) Rosenberg, E. S.; Dufort, E. M.; Udo, T.; Wilberschied, L. A.; Kumar, J.; Tesoriero, J.; Weinberg, P.; Kirkwood, J.; Muse, A.; DeHovitz, J. Association of treatment with hydroxychloroquine or azithromycin with in-hospital mortality in patients with COVID-19 in New York State. *JAMA* **2020**, *323*, 2493–2502.
- (21) Furtado, R. H. M.; Berwanger, O.; Fonseca, H. A.; Corrêa, T. D.; Ferraz, L. R.; Lapa, M. G.; Zampieri, F. G.; Veiga, V. C.; Azevedo, L. C.; Rosa, R. G. Azithromycin in addition to standard of care versus standard of care alone in the treatment of patients admitted to the hospital with severe COVID-19 in Brazil (COALITION II): a randomised clinical trial. *Lancet* **2020**, *396*, 959–967.
- (22) Zanni, R.; Galvez-Llompant, M.; Garcia-Domenech, R.; Galvez, J. Latest advances in molecular topology applications for drug discovery. *Expert Opin. Drug Discov.* **2015**, *10*, 945–957.
- (23) Sajib, A. Repurposing of Approved Drugs with Potential to Block SARS-CoV-2 Surface Glycoprotein Interaction with Host Receptor. *Preprints* **2020**, 2020040369.
- (24) Garle, M. J.; Fentem, J. H.; Fry, J. R. In vitro cytotoxicity tests for the prediction of acute toxicity in vivo. *Toxicol. In Vitro* **1994**, *8*, 1303–1312.
- (25) Kirst, H. A. Introduction to the macrolide antibiotics. In *Macrolide antibiotics*; Springer: 2002; 1–13.
- (26) Tyteca, D.; Van Der Smissen, P.; Van Bambeke, F.; Leys, K.; Tulkens, P. M.; Courtoy, P. J.; Mingeot-Leclercq, M. Azithromycin, a lysosomotropic antibiotic, impairs fluid-phase pinocytosis in cultured fibroblasts. *Eur. J. Cell Biol.* **2001**, *80*, 466–478.
- (27) Tyteca, D.; Van Der Smissen, P.; Mettlen, M.; Van Bambeke, F.; Tulkens, P. M.; Mingeot-Leclercq, M.; Courtoy, P. J. Azithromycin, a lysosomotropic antibiotic, has distinct effects on fluid-phase and receptor-mediated endocytosis, but does not impair phagocytosis in J774 macrophages. *Exp. Cell Res.* **2002**, *281*, 86–100.
- (28) Gastaminza, P.; Whitten-Bauer, C.; Chisari, F. V. Unbiased probing of the entire hepatitis C virus life cycle identifies clinical compounds that target multiple aspects of the infection. *Proc. Natl. Acad. Sci.* **2010**, *107*, 291–296.
- (29) Mingorance, L.; Friesland, M.; Coto-Llerena, M.; Pérez-del-Pulgar, S.; Boix, L.; López-Oliva, J. M.; Bruix, J.; Forn, X.; Gastaminza, P. Selective inhibition of hepatitis C virus infection by hydroxyzine and benzotropine. *Antimicrob. Agents Chemother.* **2014**, *58*, 3451–3460.
- (30) Arikata, M.; Itoh, Y.; Shichinohe, S.; Nakayama, M.; Ishigaki, H.; Kinoshita, T.; Le, M. Q.; Kawaoka, Y.; Ogasawara, K.; Shimizu, T. Efficacy of clarithromycin against H5N1 and H7N9 avian influenza A virus infection in cynomolgus monkeys. *Antiviral Res.* **2019**, *171*, No. 104591.
- (31) Kanatani, M. S.; Guglielmo, B. J. The new macrolides. Azithromycin and clarithromycin. *West. J. Med.* **1994**, *92*, 31–282.
- (32) Tiwari, V.; Beer, J. C.; Sankaranarayanan, N. V.; Swanson-Mungerson, M.; Desai, U. R. Discovering small-molecule therapeutics against SARS-CoV-2. *Drug Discovery Today* **2020**, 1535.
- (33) Huang, F.; Li, Y.; Leung, E. L.; Liu, X.; Liu, K.; Wang, Q.; Lan, Y.; Li, X.; Yu, H.; Cu, L. A review of therapeutic agents and Chinese herbal medicines against SARS-CoV-2 (COVID-19). *Pharmacol. Res.* **2020**, *158*, No. 104929.
- (34) Jeong, G. U.; Song, H.; Yoon, G. Y.; Kim, D.; Kwon, Y.-C. Therapeutic strategies against COVID-19 and structural characterization of SARS-CoV-2: a review. *Front. Microbiol.* **2020**, *11*, No. 1723.
- (35) Olah, M.; Oprea, T. I. Comprehensive Medicinal Chemistry II vol 3. Taylor, J. B.; Trigg, D. J. (eds). *Bioactivity Databases*. 2006.
- (36) Tandon, R.; Sharp, J. S.; Zhang, F.; Pomin, V. H.; Ashpole, N. M.; Mitra, D.; McCandless, M. G.; Jin, W.; Liu, H.; Sharma, P. Effective inhibition of SARS-CoV-2 entry by heparin and enoxaparin derivatives. *J. Virol.* **2021**, *95*, e01987–e01920.
- (37) Hoffmann, M.; Schroeder, S.; Kleine-Weber, H.; Müller, M. A.; Drosten, C.; Pöhlmann, S. Nafamostat mesylate blocks activation of SARS-CoV-2: new treatment option for COVID-19. *Antimicrob. Agents Chemother.* **2020**, *64*, e00754–e00720.
- (38) Sen Gupta, P. S.; Biswal, S.; Panda, S. K.; Ray, A. K.; Rana, M. K. Binding mechanism and structural insights into the identified protein target of COVID-19 and importin- $\alpha$  with in-vitro effective drug ivermectin. *J. Biomol. Struct. Dyn.* **2020**, 1–10.
- (39) Bagheri, M.; Niavarani, A. Molecular dynamics analysis predicts ritonavir and nalmoxol strongly block the SARS-CoV-2 spike protein-hACE2 binding. *J. Biomol. Struct. Dyn.* **2020**, 1–10.
- (40) Abhinand, C. S.; Nair, A. S.; Krishnamurthy, A.; Oommen, O. V.; Sudhakaran, P. R. Potential protease inhibitors and their combinations to block SARS-CoV-2. *J. Biomol. Struct. Dyn.* **2020**, 1–15.
- (41) Mauri, A. alvaDesc: A tool to calculate and analyze molecular descriptors and fingerprints. In *Ecotoxicological QSARs*; Springer: 2020; 801–820, DOI: 10.1007/978-1-0716-0150-1\_32.
- (42) Solberg, H. E. Discriminant analysis. *CRC Crit. Rev. Clin. Lab. Sci.* **1978**, *9*, 209–242.
- (43) Furnival, G. M.; Wilson, R. W. Regressions by leaps and bounds. *Technometrics* **2000**, *42*, 69–79.
- (44) Sanchez-Pinto, L. N.; Venable, L. R.; Fahrenbach, J.; Churpek, M. M. Comparison of variable selection methods for clinical predictive modeling. *Int. J. Med. Inf.* **2018**, *116*, 10–17.
- (45) Mathai, N.; Chen, Y.; Kirchmair, J. Validation strategies for target prediction methods. *Brief. Bioinformatics* **2020**, *21*, 791–802.
- (46) Statsoft, I. *STATISTICA (data analysis software system). Version 2012*, 10.
- (47) Cervantes-Barragan, L.; Züst, R.; Maier, R.; Sierro, S.; Janda, J.; Levy, F.; Speiser, D.; Romero, P.; Rohrlach, P. S.; Ludewig, B.; Thiel, V. Dendritic cell-specific antigen delivery by coronavirus vaccine vectors induces long-lasting protective antiviral and antitumor immunity. *MBio* **2010**, *1*, e00171–e00110.
- (48) Reed, L. J.; Muench, H. A simple method of estimating fifty per cent endpoints. *Am. J. Epidemiol.* **1938**, *27*, 493–497.
- (49) Corman, V. M.; Landt, O.; Kaiser, M.; Molenkamp, R.; Meijer, A.; Chu, D. K.; Bleicker, T.; Brünink, S.; Schneider, J.; Schmidt, M. L. Detection of 2019 novel coronavirus (2019-nCoV) by real-time RT-PCR. *Eurosurveillance* **2020**, *25*, No. 2000045.
- (50) Gong, E. Y.; Smets, A.; Verheyen, N.; Clynhens, M.; Gustin, E.; Lory, P.; Kraus, G. A duplex real-time RT-PCR assay for profiling inhibitors of four dengue serotypes. In *Antiviral Methods and Protocols*; Springer: 2013; 195–203.
- (51) Bartosch, B.; Dubuisson, J.; Cosset, F.-L. Infectious hepatitis C virus pseudo-particles containing functional E1–E2 envelope protein complexes. *J. Exp. Med.* **2003**, *197*, 633–642.